

REVISION 4

Revisiting the crystal structure of dickite: X-ray diffraction, solid-state NMR and DFT calculations study

JOÃO ROCHA^{1*}, FILIPE A. ALMEIDA PAZ¹, MARIANA SARDO¹, LUÍS MAFRA¹

¹University of Aveiro, Department of Chemistry, CICECO-Aveiro Institute of Materials, 3810-193 Aveiro, Portugal

ABSTRACT

Dickite is a member of the family of 1:1 dioctahedral phyllosilicates known as the kaolin minerals, with composition $\text{Al}_2\text{Si}_2\text{O}_5(\text{OH})_4$. The elucidation of the hydrogen-atom positions in dickite, addressed here, and indeed in other hydrated minerals poses particular challenges.

The crystal structure of dickite was determined from single-crystal X-ray diffraction at 100(2) K in the non-centrosymmetric *Cc* monoclinic space group and found to agree closely with previously reported structures (Bish and Johnston 1993; Dera et al. 2003). ²⁷Al and ²⁹Si solid-state NMR spectra of unprecedented resolution bear evidence for two distinct Al and Si sites, being consistent with the previously determined structures. Positions of the four independent hydrogen atoms were optimized and the pertinent ¹H chemical shifts calculated using DFT methods (program CASTEP) and compared with high-resolution MAS NMR experimental data obtained at ultra-high sample spinning rates (up to 67 kHz). This work contributes new evidence on the precise hydrogen-atom positions of dickite, and illustrates how X-ray diffraction, solid-state NMR and theoretical calculations may be combined to yield an improved mineral crystal structure.

Keywords: Dickite; crystal structure, X-ray diffraction, ¹H, ²⁷Al, ²⁹Si MAS NMR; DFT methods

INTRODUCTION

An outstanding problem in the characterisation of the crystal structure of clay minerals is the precise solution of the hydrogen-atom positions. This is mainly due to the very weak X-ray scattering power, to the presence of stacking disorder and, when neutron diffraction is used, to strong incoherent scattering from the two possible ^1H nuclear spin states. A technique complementary to diffraction methods, solid-state NMR, is very sensitive to the local structure, through the variation of interactions such as the chemical shielding, J-coupling or quadrupolar coupling providing an ideal tool for structural investigation of minerals (Ashbrook and Dawson 2016). Theoretical calculations have also been used to assist in ascertaining the hydrogen-atom positions of clay minerals (Liang and Hawthorne 1998) and references therein).

Precise determination of hydrogen positions in dickite have been the subject of many studies, mainly due to some conflicting results obtained by X-ray and neutron diffraction, infrared spectroscopy and theoretical calculations (see, *e.g.*, (Gupta et al. 1984; Bish and Johnston 1993; Liang and Hawthorne 1998; Dera et al. 2003). Here, we revisit the structure of dickite and determine the H-, Si-, Al- atom positions using a combination of X-ray diffraction, solid-state NMR and theoretical calculations. The general approach used is the following. First, the position of O, Al and Si atoms is ascertained by single crystal X-ray diffraction. With this model in hand, the H-atom positions are optimized, and the NMR chemical shifts calculated using DFT methods (program CASTEP) and compared with very high-resolution ^1H solid-state NMR experimental data. The final crystal structure consists, thus, on the positions of O, Al and Si atoms derived from X-ray diffraction, and H-atom positions geometrically optimized by DFT and validated by ^1H MAS NMR. In contrast with a previous theoretical calculations account (but in accord with other experimental reports), we have found evidence for four, rather than six, independent H-atoms (Liang and Hawthorne 1998).

EXPERIMENTAL METHODS

Single-crystal X-ray diffraction

Single crystals of a naturally occurring dickite from Anglesey (same sample as in (Adams and Jefferson 1976) were manually selected from crystalline aggregates and immersed in highly viscous FOMBLIN Y perfluoropolyether vacuum oil (LVAC 140/13, Sigma-Aldrich) (Kottke and Stalke 1993). Crystals were mounted on a Hampton Research CryoLoop with the help of a Stemi 2000 stereomicroscope equipped with Carl Zeiss lenses. X-ray diffraction data were collected at 100(2) K on a Bruker X8 Kappa APEX II charge-coupled device (CCD) area-detector diffractometer (Mo K α graphite-monochromated radiation, $\lambda = 0.7107 \text{ \AA}$) controlled by the APEX2 software package, (“APEX2 - Data Collection Software” 2006) and an Oxford Instruments Cryostrem 700 Series low-temperature device monitored remotely by the software interface Cryopad (“Cryopad, Remote monitoring and control” 2006). Diffraction images were processed using the software package SAINT+, (“SAINT+, Data integration Engine”) and data were corrected for absorption by the multiscan semi-empirical method implemented in SADABS (Sheldrick 2012). The non-H structure was solved using the algorithm implemented in SHELXT-2014, (Sheldrick 2014b) which enabled the immediate location of almost all the heaviest atoms in the asymmetric unit. The remaining missing and misplaced non-hydrogen atoms were found from difference Fourier maps calculated from successive full-matrix least-squares refinement cycles on F^2 using the latest SHELXL from the 2014 release (Sheldrick 2008, 2014a). All non-hydrogen atoms were successfully refined for their positions and the respective independent anisotropic displacement parameters. Site occupancies were fixed. All structure refinements were performed using the graphical interface ShelXle (Hübschle et al. 2011).

Even though the four crystallographically independent hydrogen atoms associated with the bridging and terminal hydroxyl groups could be directly located from difference Fourier maps, in the final structural model these atoms were placed in fixed positions, which were derived from

high-resolution solid-state NMR and theoretical calculations (see dedicated Experimental Section, for additional details). Besides the AFIX 1 instruction used in SHELXL to fix the atomic coordination of the hydrogen atoms, their isotropic thermal displacements parameters (U_{iso}) were also fixed at $1.5 \times U_{\text{eq}}$ of the parent oxygen atoms.

The oxidation state of the two crystallographically independent Al^{3+} centers was investigated using PLATON (Spek 1990, 2003) and based on the valences of all the Al–O interactions (using the measured bond distances) following the theoretical models of Brese & O’Keeffe (Brese and O’Keeffe 1991) and Brown & Altermatt (Brown and Altermatt 1985). The sums of the bond valence (considering a +3 oxidation state) were +2.81 and +2.82 for Al1 and Al2, respectively, indicating a +3 metal oxidation state.

The last difference Fourier map synthesis showed the highest peak ($0.300 \text{ e}\text{\AA}^{-3}$) and the deepest hole ($-0.482 \text{ e}\text{\AA}^{-3}$) at 0.69 and 1.61 Å from O4 and O9, respectively. The Flack parameter refined to 0.06(3) (Flack and Bernardinelli 2000).

Table 1 summarizes the data collection and structure refinement information and Table 2 lists the fractional atomic coordinates of dickite. Bond lengths and angles for tetrahedral Si^{4+} and octahedral Al^{3+} , and hydrogen bonding geometrical details are provided in Tables 3 to 5. Structural drawings have been created with software package Crystal Impact Diamond (Brandenburg 2017).

Further details of the crystal structure investigation may be obtained from FIZ Karlsruhe, 76344 Eggenstein-Leopoldshafen, Germany (Fax: (+49)7247-808-666; e-mail: crysdata@fiz-karlsruhe.de, on quoting the deposition number CSD-431456).

Solid-state NMR spectroscopy

^1H , ^{29}Si and ^{27}Al magic-angle spinning (MAS) NMR spectra were recorded, at room temperature, on a Bruker Avance III, 700 MHz (16.4 T) narrow-bore spectrometer at ^1H , ^{29}Si and ^{27}Al Larmor frequencies of 700.1, 139.1 and 182.4 MHz, respectively. ^{29}Si cross-polarization (CP) MAS, ^{27}Al MAS and ^{27}Al triple-quantum (3Q) MAS NMR spectra were recorded on a triple-resonance 2.5 mm Bruker probe with 10–14 kHz spinning rates. ^1H MAS NMR spectra were

recorded on a triple-resonance 1.3 mm Bruker probe with a spinning rate of 67 kHz, a recycle delay of 120 s, and a 90° pulse corresponding to a radio-frequency (RF) field strength of 139 kHz.

Acquisition parameters for the ^{29}Si CPMAS experiment were the following: ^1H and ^{29}Si 90° pulses were set to 2 and 6 μs , corresponding to a RF field strength of 125 and 42 kHz, respectively. The CP step was implemented using a contact time of 2 ms with a ramp shape in the ^1H channel of 50-100% and ^{29}Si RF field strength of 66 kHz. During the acquisition, SPINAL-64 (Fung et al. 2000) decoupling with a RF field strength of 50 kHz (SPINAL basic pulse length of 9.5 μs) was employed.

^{27}Al MAS NMR spectra were recorded using a short RF pulse of 0.16 μs (equivalent to a $\pi/18$ flip angle), calibrated on an aqueous solution of $\text{Al}(\text{NO}_3)_3$, employing a RF field strength of 174 kHz and 2 s recycle delay. ^{27}Al 3QMAS NMR experiments were performed using the split- t_1 z-filter pulse sequence (Brown et al. 1996) using RF pulse lengths of 2 μs and 0.8 μs for the first two hard pulses, and a 16 μs 90° soft pulse. RF field strengths of 179 and 5 kHz were used for the hard and soft pulses, respectively. 105 t_1 points were acquired in the indirect dimension with 4368 scans each, using a recycle delay of 0.5 s.

Chemical shifts are quoted in ppm from TMS (0 ppm), Q8M8 (-109.68 ppm, for the farthest downfield frequency peak) and aqueous solution of $\text{Al}(\text{NO}_3)_3$ (0 ppm) for ^1H , ^{29}Si , and ^{27}Al , respectively. Simulations of the NMR spectra were carried out using the program dmfit (Massiot et al. 2002).

COMPUTATIONAL METHODS

DFT calculation of NMR chemical shieldings was performed using the plane wave pseudopotential formalism and the generalized gradient approximation (GGA) Perdew, Burke, and Ernzerhof (PBE) exchange correlation functional (Perdew et al. 1996). All calculations were carried out with the CASTEP code (Clark et al. 2005) on a Linux workstation with 64 Gb RAM (2133 MHz ECC DDR4); dual socket Intel Xeon processor E5-2650 v 3 family @ 2 GHz using 16

cores with 2 threads in each core (hyper-threading); QPI up to 9.6 GT/s, and employing ultrasoft pseudopotentials calculated on-the-fly. The gauge including projector augmented wave (GIPAW) approach (Pickard and Mauri 2001) was employed, allowing chemical shifts to be calculated with an all-electron accuracy within the pseudopotential framework.

The starting structure of dickite was obtained from single-crystal X-ray diffraction. Using CASTEP, an optimization of hydrogen atom positions was conducted at fixed unit cell, reaching full convergence after 11 Broyden-Fletcher-Goldfarb-Shanno (BFGS) geometry optimization iteration cycles; plane-wave basis set cutoff energy of 700 eV; Brillouin zone was sampled with a $4 \times 3 \times 2$ Monkhorst-Pack (MP) k-point grid size for SCF calculations (k-point spacing of 0.05 \AA^{-1}); 8k-points were used. Total energy atom convergence tolerance was set to 1×10^{-8} eV; size of fine grid of 3. All other CASTEP geometry convergence criteria were set to their default values. After full geometry optimization, ^1H and ^{27}Al isotropic chemical shieldings, and ^{27}Al quadrupolar parameters were calculated using the basis set cutoff and MP grid mentioned above. Calculated isotropic chemical shieldings (σ_{iso}) were converted to isotropic chemical shifts (δ_{iso}), as follows:

$$\delta_{iso} = (\sigma_{iso} - \sigma_{ref}) / m \quad (1)$$

where σ_{ref} and m are the y-intercept and slope, respectively, of the linear regression obtained by plotting σ_{iso} against the measured isotropic chemical shifts (δ_{iso}). The linearity of Equation 1 ensures that the spectral assignment can be done, avoiding ambiguities.

RESULTS AND DISCUSSION

Single-Crystal X-ray Diffraction

The crystal structure of dickite was determined from single-crystal X-ray diffraction studies at 100(2) K in the non-centrosymmetric *Cc* monoclinic space group, in exact agreement with the structures previously reported (Dera et al. 2003). In the Supporting Information we provide tabulated fractional coordinates and hydrogen bonding geometries of four structure determinations of dickite, including that of the present one. There is excellent agreement between these structures,

particularly in what concerns the non-hydrogen backbone. Some differences are, however, observed in the location of the hydrogen atoms, as witnessed by the hydrogen bonding interactions: while the structures of Dera et al., Mercier and Le Page and the present one, evidence an intra-layer O–H···O interactions (see below), the structure of Bish and Johnston does not show such interactions. The remaining geometries for the inter-layer interactions are similar (note that the structures were collected at different temperatures).

The 1:1 layer in the crystal structure of dickite consists of two pairs of crystallographically independent {SiO₄} and {AlO₆} polyhedra. Two {SiO₄} tetrahedra are very similar: in Si1, the Si–O distances and internal O–Si–O angles range from, respectively 1.6024(14) to 1.6202(12) Å [Δ = 0.0178 Å] and 105.63(6) to 113.99(7)° [Δ = 8.36°]; in Si2, the respective values are 1.6077(15)–1.6256(12) [Δ = 0.0179 Å] and 106.07(7)–113.35(7)° [Δ = 7.28°] (Table 2). Remarkably, the main difference between these two independent {SiO₄} tetrahedra is found in the internal tetrahedral angles, for Si1 the angle interval [Δ] is *ca.* 15% larger than for Si2. Concerning the two {AlO₆} octahedra, it is the inter-atomic distances that differ significantly. Indeed, although Δ values are almost identical (Δ 2.51°/21.58° and 2.44°/21.77° for the *trans/cis* angles of Al1 and Al2, respectively), the dispersion of Al–O distances is significant: Al1, 1.8537(16)–2.0003(13) Å range [Δ = 0.1474 Å]; Al2, 1.8534(15)–1.9898(13) Å range [Δ = 0.1356 Å] (Table 3).

As found in previous structural determinations, (Dera et al. 2003) the dickite neutral layers close pack along the [001] direction, mediated by the hydrogen bond networks involving the hydroxyl groups (Figure 1). From a supramolecular point of view, these neutral layers consist of two sub-units with different roles (Figures 2 and 3). Al–Al bridging hydroxyl groups O6, O7 and O8 establish connections with the neighbouring layer via strong [$d(D\cdots A)$ distances between 2.9313(19) and 3.1236(19) Å] and directional (interaction angles up to 166°) O–H···O bonds (Figure 3 and Table 4). Within the layer, there is a bifurcated interaction involving the hydroxyl group O9. Both, the internuclear distances (larger than *ca.* 3.4 Å), and the interaction angles (*ca.* 140°), witness a significantly weaker interaction, reflecting its bifurcated nature (Figure 3).

Solid-state NMR

In accord with the crystal structure of dickite, which calls for the presence of two crystallographically non-equivalent Si-sites, the ^{29}Si CPMAS spectrum (Figure 4) consists of two narrow (18.3 Hz full-width-at-half-maximum) resonances at -91.0 and -91.5 ppm, characteristic of layered silicates and assigned to Q^3 , *i.e.*, $\text{Si}-(\text{OSi})_3\text{O}$, environments. This attribution is consistent with previous studies, as is the observation of two resonances separated by *ca.* 0.5 ppm (Barron et al. 1983). To the best of our knowledge, no other study of kaolin minerals reports ^{29}Si NMR spectra of such high resolution (Rocha and Klinowski 1990).

^{27}Al (a spin 5/2 nucleus) quadrupole moment interacts with the electric field gradients (EFG) generated by the surrounding electronic cloud. Although this interaction broadens the ^{27}Al spectrum it also yields valuable information on local site symmetry. Quadrupolar interaction is described by the quadrupole coupling constant, $C_Q = e^2qQ/h$, and the asymmetry parameter, $\eta_Q = (V_{xx} - V_{yy})/V_{zz}$, where eQ is the electric nuclear quadrupole moment, and $eq = V_{zz}$ is the largest eigenvalue (in magnitude) of the EFG tensor \mathbf{V} .

The simulated ^{27}Al MAS NMR spectrum of dickite (Figure 5) exhibits two overlapping central transition resonances (Al1 and Al2) at *ca.* 5.3 ppm, given by two crystallographically distinct six-coordinated Al sites revealed by X-ray diffraction. The two resonances were determined by restraining the Al1/Al2 ratio to 1, using the quadrupolar parameters C_Q and η_Q obtained from GIPAW-DFT (Table 5), and the isotropic chemical shift values, δ_{iso} , calculated using Equation 2 (Massiot et al. 2002):

$$\delta_{iso} = \delta_{CG} + \delta_{QIS} \quad (2)$$

where δ_{CG} is the centre of gravity of the line, and δ_{QIS} the second-order quadrupolar-induced shift:

$$\delta_{QIS} = Coeff \times \left(\frac{C_Q}{\nu_{Larmor}} \right)^2 \times \left(1 + \frac{\eta_Q^2}{3} \right) \quad (3)$$

with $Coeff = 6000$ for $I=5/2$ (^{27}Al).

Calculated chemical shieldings ($\sigma_{\text{iso}}^{\text{Al1}} = 546.19$ ppm and $\sigma_{\text{iso}}^{\text{Al2}} = 545.28$ ppm) only differ by 0.91 ppm, a difference comparable to the isotropic chemical shifts of the two Al sites, $\Delta\delta_{\text{iso}} = 0.77$ ppm, obtained from spectral fitting (Figure 5 and Table 1).

In general, DFT calculations of isotropic chemical shifts have a precision of a few ppm (Bonhomme et al. 2012), while the precision of the calculations of ^{27}Al quadrupolar coupling constants in aluminosilicates is often less than 0.5 MHz (Rocquefelte et al. 2007; Vyalikh et al. 2010). It is thus remarkable that the dickite calculations reported here (which allow a very good simulation of the ^{27}Al MAS NMR spectrum) yielded differences between C_Q and δ_{iso} values for both Al sites of less than 0.2 MHz and 1 ppm, respectively. A previous kaolinite study by satellite transition MAS NMR spectroscopy found evidence for two ^{27}Al resonances with C_Q and δ_{iso} values differing, respectively, 0.64 MHz and 1.1 ppm. However, these figures were based on an approximate model (Rocha and Pedrosa de Jesus 1994). A more recent study, yielded the following parameters for the two sites: $\delta_{\text{iso}} = 7.5$ ppm, $C_Q = 3.4$ MHz, $\eta_Q = 0.8$, and $\delta_{\text{iso}} = 8.0$ ppm, $C_Q = 3.0$ MHz, $\eta_Q = 0.9$ (Paris 2014). These values are in good agreement with those reported in the present work.

Given the similitude of the quadrupole coupling parameters and the isotropic chemical shifts of the two Al-sites, it is not possible to resolve two resonances even in the ^{27}Al 3QMAS NMR spectrum (Figure 6). However, the spectrum is informative because it shows that there is essentially no distribution of chemical shifts and quadrupolar parameters (ascertained along the CS and QIS axes in Figure 6), indicating the absence of any significant Al-site disorder.

Consider the high-resolution ^1H MAS NMR spectra of dickite in Figure 7. Although the spectrum recorded with a 67 kHz spinning rate (1.3 mm rotors) displays an improved resolution revealing, in particular, two resonances at 1.9 and 2.2 ppm, it was not used for spectral decomposition purposes due to significant probe background. A spectrum recorded at 35 kHz (2.5

mm rotor) was used, instead. The four distinct ^1H resonances at *ca.* 1.90 ppm H(9'), 2.20 ppm H(7'), 3.10 ppm H(8') and 3.40 ppm H(6'), on a *ca.* 1:1:1:1 intensity ratio, are consistent with the X-ray diffraction evidence. Figures 2 and 3 show that two AlOH hydrogen atoms are engaged in considerably shorter hydrogen bonding interactions [Al-O(6)H \cdots O(4) ($d_{\text{H}\cdots\text{O}} \approx 1.982 \text{ \AA}$) and Al-O(8)H \cdots O(1) ($d_{\text{H}\cdots\text{O}} \approx 1.981 \text{ \AA}$)] than the other two hydrogen atoms [Al-O(9)H \cdots O(2) ($d_{\text{H}\cdots\text{O}} \approx 2.635 \text{ \AA}$); Al-O(7)H \cdots O(3) ($d_{\text{H}\cdots\text{O}} \approx 2.331 \text{ \AA}$)]. This fact results in two sets of ^1H chemical shifts ($\delta_{\text{iso}} = 1.9 - 2.2$ and $\delta_{\text{iso}} = 3.1 - 3.4$). GIPAW-DFT calculations and experimental ^1H chemical shifts (Table 6 and Figure 8) are in very good agreement, hence supporting the resonance assignment and validating the DFT-optimized structure model. Liang and Hawthorne (Liang and Hawthorne 1998) calculated proton positions using the static structure-energy minimization approach and concluded that the theoretical and experimental results agreed poorly, using the space group Cc. The authors have then determined proton positions in dickite with *P1* symmetry projected back into the asymmetric unit of the Cc space group and, instead of representing all four H atoms as occupying single sites, two were placed in split sites accounting for a total of six distinct OH protons. This was also in accord with the presence of six decomposed infrared spectroscopy (IR) OH stretching bands. (Liang and Hawthorne 1998) However, the IR and Raman spectra could also be decomposed in only four bands. (Balan et al. 2005) It is worth mentioning that OH \cdots H hydrogen bond distances retrieved from different sources are considerably different because H positions were usually determined based on empiric approaches (Liang and Hawthorne 1998; Balan et al. 2005) and FTIR measurements (Bish and Johnston 1993). None of the previous results reported $d_{\text{H}\cdots\text{O}} \approx 2.635 \text{ \AA}$, from an intra-layer hydrogen bond (Figures 2 and 3), matching very well the most shielded ^1H environment determined experimentally ($\delta_{\text{iso}} = 1.90 \text{ ppm}$) or calculated ($\delta_{\text{iso}} = 1.94 \text{ ppm}$).

IMPLICATIONS

The crystal structure of the important mineral dickite was revisited by single-crystal X-ray diffraction, and ^1H , ^{27}Al and ^{29}Si solid-state NMR. High-resolution ^1H MAS NMR spectra recorded at ultra-high spinning rates revealed, for the first time, four resonances. This constitutes direct evidence for the presence of an equal number of distinct H-sites in dickite, independent from diffraction methods. The H-sites positions have been optimized using DFT methods and validated with NMR data, which are very sensitive to the local structure. The result is, we submit, an improved structural model of dickite, which we have confronted with three other previously reported models. The main ideas of the method presented here for determining the H-atom positions may be extended to further minerals, in particular other $\text{Al}_2\text{Si}_2\text{O}_5(\text{OH})_4$ polymorphs, kaolinite, halloysite, and nacrite. The hydrogen bond network present in dickite determines a number of important processes, such as grafting and intercalation of molecules, composite formation, and thermal transformation (dehydroxylation). The improved structural model proposed here will assist in better understanding dickite's structure-properties relationships.

ACKNOWLEDGMENTS

We are indebt to Dr. John M. Adams for his kind offer of the dickite specimen. We thank Dr. J Richard Gomes for assistance in preparing table S1. We wish to thank Fundação para a Ciência e a Tecnologia (FCT, Portugal), the European Union, QREN, FEDER through *Programa Operacional Factores de Competitividade* (COMPETE), and CICECO - Aveiro Institute of Materials, POCI-01-0145-FEDER-007679 (FCT Ref. UID/CTM/50011/2013), financed by national funds through the FCT/MEC and when appropriate co-financed by FEDER under the PT2020 Partnership Agreement. The authors are also grateful to the Portuguese NMR Network (RNRMN).

REFERENCES

- Adams, J.M., and Jefferson, D.A. (1976) The crystal structure of a dickite: formamide intercalate $\text{Al}_2\text{Si}_2\text{O}_5(\text{OH})_4\cdot\text{HCONH}_2$. *Acta Crystallographica Section B Structural Crystallography and Crystal Chemistry*, 32, 1180–1183.
- APEX2 - Data Collection Software (2006). Bruker AXS, Delft, The Netherlands.
- Ashbrook, S.E., and Dawson, D.M. (2016) NMR spectroscopy of minerals and allied materials. In *Nuclear Magnetic Resonance Vol. 45*, pp. 1–52. Royal Society of Chemistry.
- Balan, E., Lazzeri, M., Saitta, A.M., Allard, T., Fuchs, Y., and Mauri, F. (2005) First-principles study of OH-stretching modes in kaolinite, dickite and nacrite. *American Mineralogist*, 90, 50–60.
- Barron, P.F., Frost, R.L., Skjemstad, J.O., and Koppi, A.J. (1983) Detection of two silicon environments in kaolins by solid-state ^{29}Si NMR. *Nature*, 302, 49–50.
- Bish, D.L., and Johnston, C.T. (1993) Rietveld refinement and Fourier-transform infrared spectroscopic study of the dickite structure at low temperature. *Clays and Clay Minerals*, 41, 297–304.
- Bonhomme, C., Gervais, C., Babonneau, F., Coelho, C., Pourpoint, F., Azais, T., Ashbrook, S.E., Griffin, J.M., Yates, J.R., Mauri, F., and others (2012) First-principles calculation of NMR parameters using the gauge including projector augmented wave method: a chemist's point of view. *Chemical Reviews*, 112, 5733–5779.
- Brandenburg, K. (2017) DIAMOND. Crystal Impact GbR, Bonn, Germany.
- Brese, N.E., and O'Keeffe, M. (1991) Bond-valence parameters for solids. *Acta Crystallographica Section B Structural Science*, 47, 192–197.
- Brown, I.D., and Altermatt, D. (1985) Bond-valence parameters obtained from a systematic analysis of the Inorganic Crystal Structure Database. *Acta Crystallographica Section B Structural Science*, 41, 244–247.
- Brown, S.P., Heyes, S.J., and Wimperis, S. (1996) Two-dimensional MAS multiple-quantum NMR of quadrupolar nuclei. Removal of inhomogeneous second-order broadening. *Journal of Magnetic Resonance*, 119, 280–284.

- Clark, S.J.J., Segall, M.D., Pickard, C.J.J., Hasnip, P.J.J., Probert, M.I.J., Refson, K., and Payne, M.C. (2005) First principles methods using CASTEP. *Zeitschrift für Kristallographie*, 220, 567–570.
- Cryopad, Remote monitoring and control (2006). Oxford Cryosystems, Oxford, UK.
- Dera, P., Prewitt, C.T., S., J., Bish, D.L., and Johnson, C.T. (2003) Pressure-controlled polytypism in hydrous layered materials. *American Mineralogist*, 88, 1428–1435.
- Flack, H.D., and Bernardinelli, G. (2000) Reporting and evaluating absolute-structure and absolute-configuration determinations. *Journal of Applied Crystallography*, 33, 1143–1148.
- Fung, B.M., Khittrin, A.K., and Ermolaev, K. (2000) An Improved Broadband Decoupling Sequence for Liquid Crystals and Solids. *Journal of Magnetic Resonance*, 142, 97–101.
- Gupta, P.K. Sen, Schlemper, E.O., Johns, W.D., and Ross, F. (1984) Hydrogen positions in dickite. *Clays and Clay Minerals*, 32, 483–485.
- Hübschle, C.B., Sheldrick, G.M., Dittrich, B., P., L., and B., D. (2011) ShelXle: a Qt graphical user interface for SHELXL. *Journal of Applied Crystallography*, 44, 1281–1284.
- Kottke, T., and Stalke, D. (1993) Crystal handling at low temperatures. *Journal of Applied Crystallography*, 26, 615–619.
- Liang, J.-J., and Hawthorne, F.C. (1998) Calculated H-atom positions in micas and clay minerals. *The Canadian Mineralogist*, 36, 1577–1585.
- Massiot, D., Fayon, F., Capron, M., King, I., Le Calvé, S., Alonso, B., Durand, J.-O., Bujoli, B., Gan, Z., and Hoatson, G. (2002) Modelling one- and two-dimensional solid-state NMR spectra. *Magnetic Resonance in Chemistry*, 40, 70–76.
- Paris, M. (2014) The two aluminum sites in the ^{27}Al MAS NMR spectrum of kaolinite: Accurate determination of isotropic chemical shifts and quadrupolar interaction parameters. *American Mineralogist*, 99, 393–400.
- Perdew, J.P., Burke, K., and Ernzerhof, M. (1996) Generalized Gradient Approximation Made Simple. *Physical Review Letters*, 77, 3865–3868.
- Pickard, C.J., and Mauri, F. (2001) All-electron magnetic response with pseudopotentials: NMR

chemical shifts. *Physical Review B*, 63, 245101-1-245101–12.

- Rocha, J., and Klinowski, J. (1990) Kaolinite as a convenient standard for setting the Hartmann-hahn match for ^{29}Si CP/MAS NMR of silicates. *Journal of Magnetic Resonance*, 90, 567–568.
- Rocha, J., and Pedrosa de Jesus, J.D. (1994) ^{27}Al satellite transition MAS-NMR spectroscopy of kaolinite. *Clay Minerals*, 29, 287–291.
- Rocquefelte, X., Clabau, F., Paris, M., Deniard, P., Le Mercier, T., Jobic, S., and Whangbo, M.-H. (2007) Resolving the aluminum ordering in aluminosilicates by a combined experimental/theoretical study of ^{27}Al electric field gradients. *Inorganic Chemistry*, 46, 5456–5458.
- SAINT+, Data integration Engine (n.d.). Bruker AXS, Madison, Wisconsin, USA.
- Sheldrick, G.M. (2008) A short history of SHELX. *Acta Crystallographica Section A Foundations of Crystallography*, 64, 112–122.
- (2012) SADABS - area detector scaling and adsorption correction. Bruker AXS, Madison, Wisconsin, USA.
- (2014a) SHELXL - program for crystal structure refinement.
- (2014b) SHELXT - program for crystal structure solution. University of Göttingen.
- Spek, A.L. (1990) PLATON, an integrated tool for the analysis of the results of a single crystal structure D determination. *Acta Crystallographica Section A Foundations of Crystallography*, 46, 34–34.
- Spek, A.L. (2003) Single-crystal structure validation with the program PLATON. *Journal of Applied Crystallography*, 36, 7–13.
- Vyalikh, A., Zesewitz, K., and Scheler, U. (2010) Hydrogen bonds and local symmetry in the crystal structure of gibbsite. *Magnetic Resonance in Chemistry*, 48, 877–881.

FIGURE CAPTIONS

FIGURE 1. Mixed ball-and-stick and polyhedral representation of the crystal packing in dickite viewed along the [100] crystallographic direction. Dashed light-blue lines depict intra- and inter-layer O–H···O hydrogen bonds. Geometrical details on the supramolecular interactions are given in Table 4.

FIGURE 2. Mixed tetrahedral-octahedral neutral layer of dickite. Dashed light-blue lines depict intra-layer O–H···O hydrogen bonds (symmetry transformations used to generate equivalent atoms are omitted for clarity). Geometrical details on the supramolecular interactions are given in Table 4. Colour scheme as in Figure 1.

FIGURE 3. Schematic view of the interlayer space of dickite. Dashed light-blue lines depict intra- and inter-layer O–H···O hydrogen bonds (symmetry transformations used to generate equivalent atoms are omitted for clarity). Geometrical details on the supramolecular interactions are given in Table 4. Colour scheme as in Figure 1.

FIGURE 4. ^{29}Si CPMAS NMR spectrum of dickite recorded at 16.4 T, with a 10 kHz spinning rate.

FIGURE 5. ^{27}Al single-pulse MAS NMR spectrum of dickite recorded at 16.4 T with a 14 kHz spinning rate. The inset depicts the simulation of the central transition spectral region: black line – experimental spectrum; red line – simulated spectrum; purple and green – individual simulation peaks. The four faint groups of signals flanking the main peak are satellite-transition spinning sidebands.

FIGURE 6. 2D ^{27}Al 3QMAS NMR spectrum of dickite recorded at 16.4 T with a spinning rate of 14 kHz. The chemical shift (CS) and the second-order quadrupole induced shift (QIS) axes are depicted by dashed arrows.

FIGURE 7. ^1H single-pulse NMR spectrum of dickite recorded at 16.4 T with a spinning rate of 35 kHz. Black line – experimental spectrum; red line – simulated spectrum; purple and green lines – individual simulation peaks. Inset shows a selected region of the ^1H NMR spectrum recorded with

a spinning rate of 67 kHz, which clearly resolves the peaks at 1.9 and 2.2 ppm. Peak depicted with ★ is absent from the 67 kHz spectrum and is ascribed to water adsorbed on the external surface of the crystals (removed by temperature increase at ultra-high spinning rate). Peaks marked with ● and ○ depict impurities.

FIGURE 8. GIPAW calculated ^1H isotropic chemical shieldings (σ_{iso}) vs. measured ^1H isotropic chemical shifts (δ_{iso}). σ_{ref} and m are the y-intercept and slope, respectively, as defined by Eq. 3 in the experimental section.

TABLES

Table 1. Crystal and structure refinement data of dickite.

Formula	Al ₂ H ₄ O ₉ Si ₂
Formula weight	258.17
Crystal system	Monoclinic
Space group	Cc
<i>a</i> /Å	5.1444(2)
<i>b</i> /Å	8.9334(3)
<i>c</i> /Å	14.3896(5)
γ ^o	96.544(2)
Volume/Å ³	656.99(4)
<i>Z</i>	4
<i>D_c</i> /g cm ⁻³	2.610
μ (Mo-K α)/mm ⁻¹	0.836
Crystal size/mm	0.18 x 0.13 x 0.06
Crystal type	Colourless blocks
θ range	4.56 to 33.10
Index ranges	$-7 \leq h \leq 7$ $-12 \leq k \leq 13$ $-22 \leq l \leq 22$
Reflections collected	15966
Independent reflections	2412 [<i>R</i> _{int} = 0.0251]
Completeness to $\theta = 25.24^\circ$	99.8%

Final R indices $[I > 2\sigma(I)]^{a,b}$	$R1 = 0.0180$
	$wR2 = 0.0467$
Final R indices (all data) ^{a,b}	$R1 = 0.0184$
	$wR2 = 0.0470$
Weighting scheme ^c	$m = 0.0254$
	$n = 0.2079$
Largest diff. peak and hole	0.300 and -0.482 eÅ ⁻³

$${}^a R1 = \frac{\sum ||F_o| - |F_c||}{\sum |F_o|}$$

$${}^b wR2 = \sqrt{\frac{\sum [w(F_o^2 - F_c^2)^2]}{\sum [w(F_o^2)^2]}}$$

$${}^c w = 1 / [\sigma^2(F_o^2) + (mP)^2 + nP] \text{ where } P = (F_o^2 + 2F_c^2) / 3$$

Table 2. Bond distances (in Å) and angles (in degrees) for the two crystallographically independent tetrahedral {SiO₄} environments present in dickite.^a

Si1–O1	1.6202(12)	O1–Si1–O4	106.04(7)
Si1–O2	1.6024(14)	O2–Si1–O1	111.84(7)
Si1–O3	1.6132(13)	O2–Si1–O3	113.99(7)
Si1–O4	1.6268(12)	O2–Si1–O4	110.99(7)
		O3–Si1–O1	107.86(7)
		O3–Si1–O4	105.63(6)
Si2–O1	1.6256(12)	O3 ⁱ –Si2–O1	106.68(7)
Si2–O3 ⁱ	1.6119(13)	O3 ⁱ –Si2–O4 ⁱⁱ	108.08(7)
Si2–O4 ⁱⁱ	1.6242(13)	O4 ⁱⁱ –Si2–O1	106.07(7)
Si2–O5	1.6077(15)	O5–Si2–O1	110.53(6)
		O5–Si2–O3 ⁱ	113.35(7)
		O5–Si2–O4 ⁱⁱ	111.75(7)

^a Symmetry transformations used to generate equivalent atoms: (i) $\frac{1}{2}+x, \frac{1}{2}+y, z$;
(ii) $-\frac{1}{2}+x, \frac{1}{2}+y, z$.

Table 3. Bond distances (in Å) and angles (in degrees) for the two crystallographically independent octahedral {AlO₆} environments present in dickite.^a

A11–O2	1.9440(13)	O2–A11–O5	89.79(6)
A11–O5	2.0003(13)	O6–A11–O2	164.00(7)
A11–O6	1.8529(14)	O6–A11–O5	75.87(5)
A11–O7	1.8551(15)	O6–A11–O7	97.87(7)
A11–O8	1.8537(16)	O6–A11–O8	97.04(7)
A11–O9	1.9198(14)	O6–A11–O9	95.85(6)
		O7–A11–O2	97.64(5)
		O7–A11–O5	166.09(7)
		O7–A11–O9	77.69(6)
		O8–A11–O2	77.29(6)
		O8–A11–O5	96.50(6)
		O8–A11–O7	96.60(6)
		O8–A11–O9	166.51(6)
		O9–A11–O2	91.25(6)
		O9–A11–O5	90.46(6)
A12–O2 ⁱⁱ	1.9898(13)	O5–A12–O2 ⁱⁱ	90.08(5)
A12–O5	1.9399(13)	O6–A12–O2 ⁱⁱ	96.52(6)
A12–O6	1.8543(15)	O6–A12–O5	77.34(6)
A12–O7 ⁱ	1.8608(15)	O6–A12–O7 ⁱ	96.28(7)
A12–O8 ⁱⁱ	1.8534(15)	O6–A12–O9 ⁱ	166.83(6)
A12–O9 ⁱ	1.9162(13)	O7 ⁱ –A12–O2 ⁱⁱ	166.14(6)
		O7 ⁱ –A12–O5	97.92(6)

O7 ⁱ -A12-O9 ⁱ	77.64(6)
O8 ⁱⁱ -A12-O2 ⁱⁱ	76.15(6)
O8 ⁱⁱ -A12-O6	96.70(6)
O8 ⁱⁱ -A12-O5	164.39(7)
O8 ⁱⁱ -A12-O7 ⁱ	97.06(6)
O8 ⁱⁱ -A12-O9 ⁱ	95.65(5)
O9 ⁱ -A12-O2 ⁱⁱ	90.87(6)
O9 ⁱ -A12-O5	91.80(6)

^a Symmetry transformations used to generate equivalent atoms: (i) $\frac{1}{2}+x, \frac{1}{2}+y, z$;
(ii) $-\frac{1}{2}+x, \frac{1}{2}+y, z$.

Table 4. Geometrical details (distances in Å and angles in degrees)

on the strong hydrogen bonds present in dickite.^a

D–H···A	<i>d</i>(D···A)	<(DHA)
O6–H6'···O4 ⁱⁱⁱ	2.9313(19)	164
O7–H7'···O3 ^{iv}	3.1236(19)	137
O8–H8'···O1 ^v	2.932(2)	166
O9–H9'···O2 ⁱⁱ	3.4349(19)	139
O9–H9'···O5 ^{vi}	3.4287(19)	140

^a Symmetry transformations used to generate equivalent atoms:

(ii) $-\frac{1}{2}+x, \frac{1}{2}+y, z$; (iii) $-\frac{1}{2}+x, 1.5-y, \frac{1}{2}+z$; (iv) $x, 1-y, \frac{1}{2}+z$;

(v) $\frac{1}{2}+x, 1.5-y, \frac{1}{2}+z$; (vi) $-1+x, y, z$.

Table 5. Quadrupolar parameters C_Q , η_Q and δ_{QIS} and isotropic chemical shift (δ_{iso}) determined for dickite's aluminium sites depicted in Figure 3. For the calculation of δ_{QIS} , $\nu_{Larmor}(^{27}\text{Al}) = 182.39$ Hz, corresponding to a 16.4 T spectrometer.

Aluminium site	C_Q^a (MHz)	η_Q^a	δ_{QIS}^b (ppm)	δ_{iso}^b (ppm)
Al 1	-3.42	0.99	2.82	8.65
Al 2	3.56	0.94	2.96	7.88

^a calculated using GIPAW-DFT; ^b calculated using Eqs. 1 and 2.

Table 6. Experimental and calculated δ_{iso} (^1H) values (ppm) of dickite.

Proton label	Exp. δ_{iso}	Calc. δ_{iso}
H9'	1.90	1.94
H7'	2.20	2.18
H8'	3.10	3.26
H6'	3.40	3.38

FIGURES

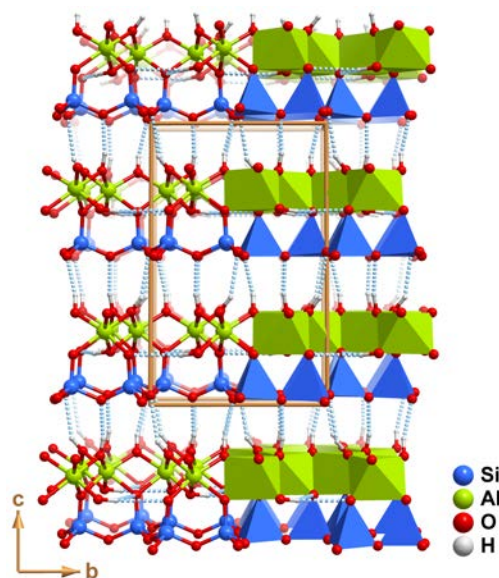


Figure 1

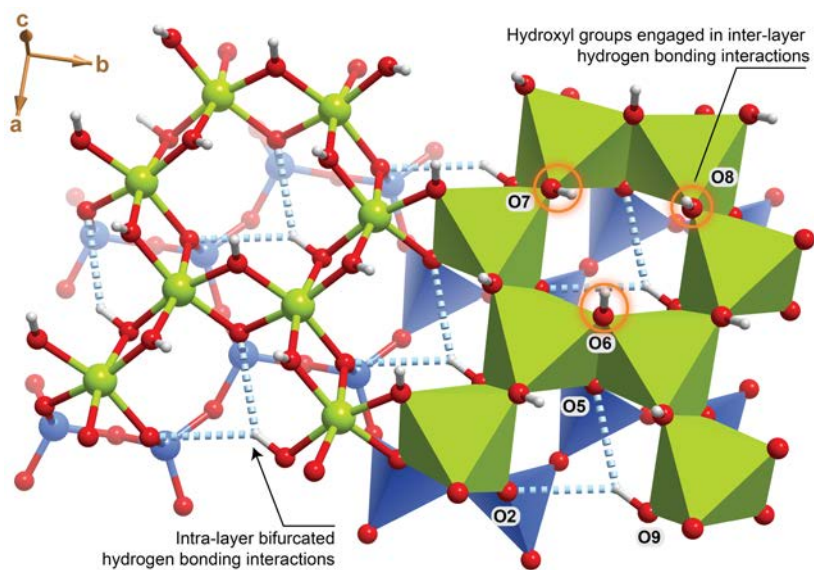


Figure 2

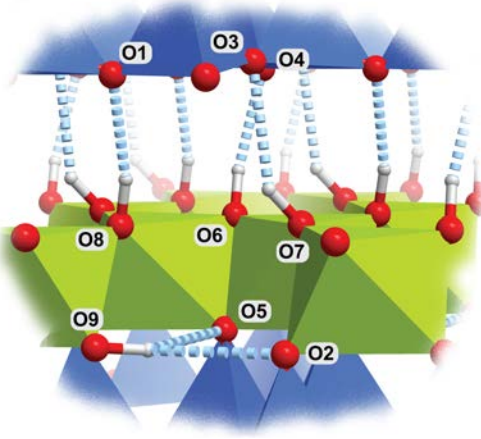


Figure 3

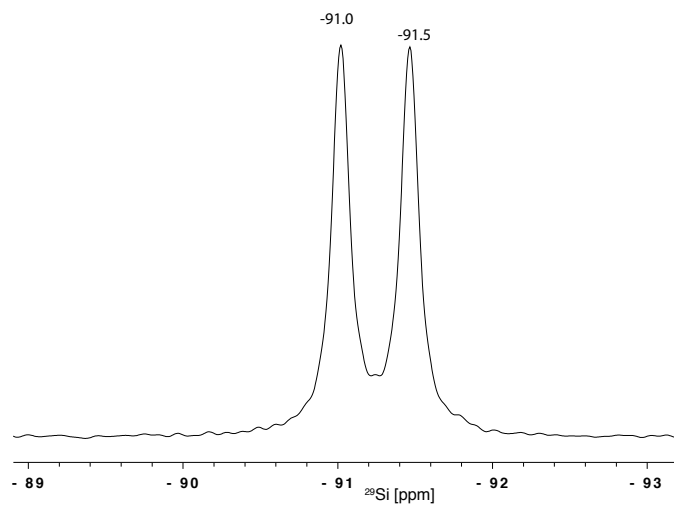


Figure 4

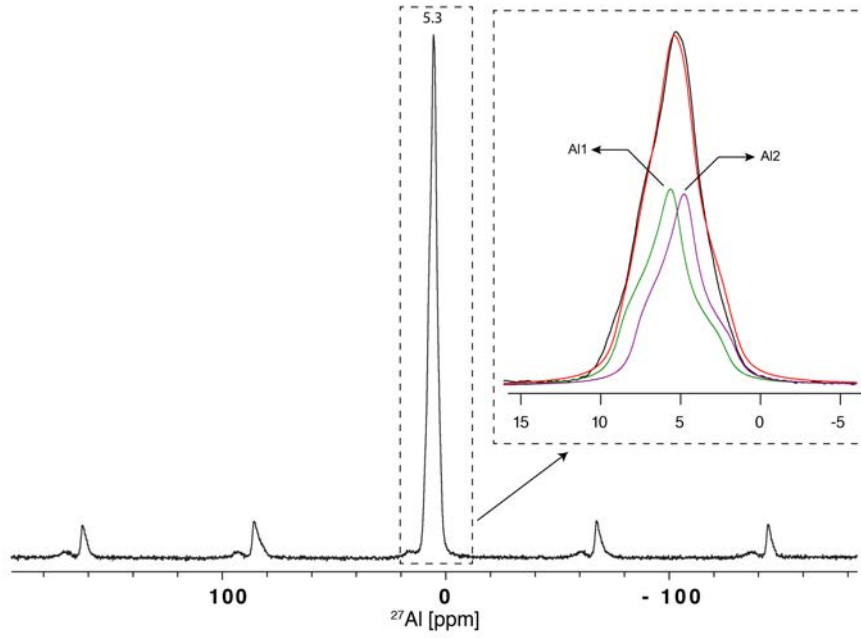


Figure 5

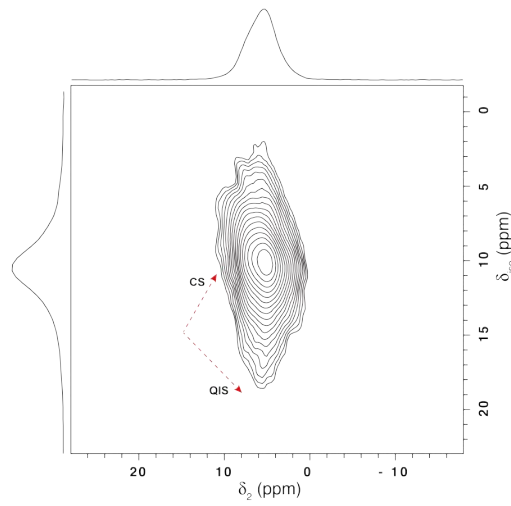


Figure 6

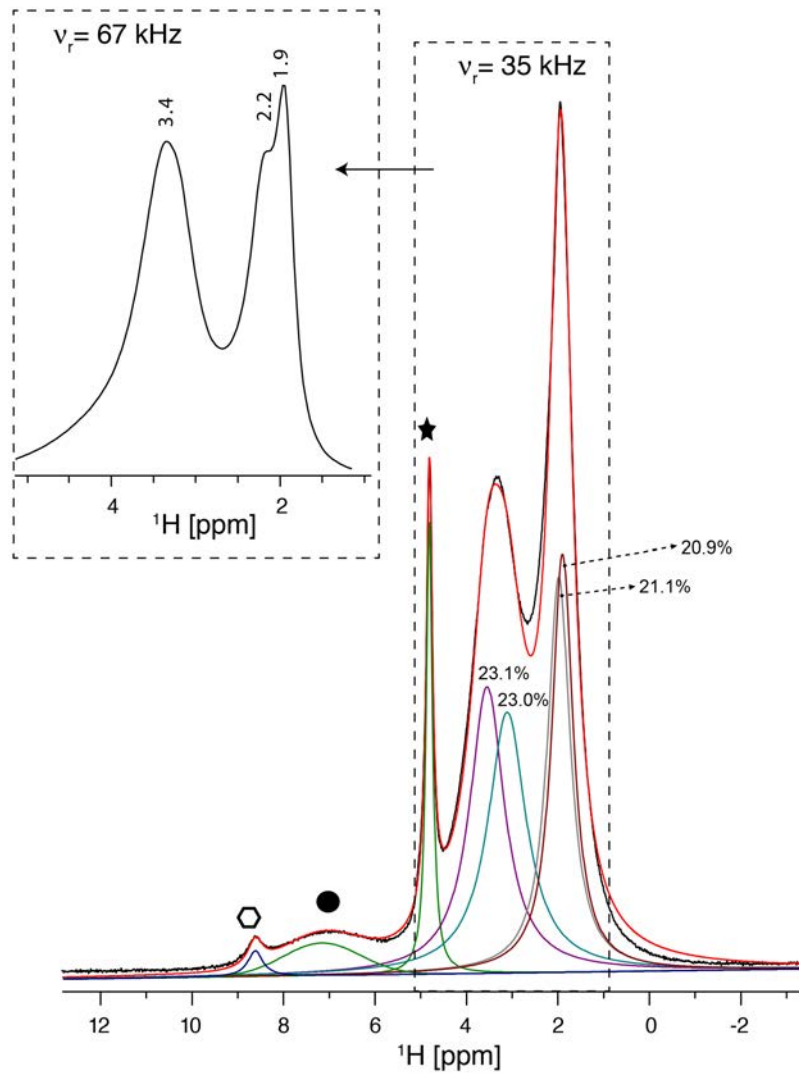


Figure 7

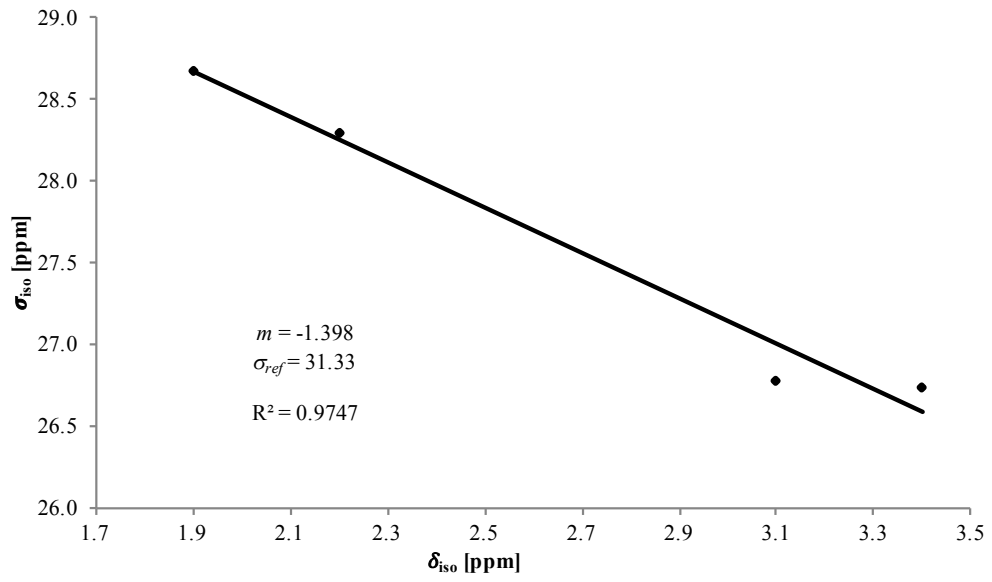


Figure 8